ARTICLE

Homolytic Cleavage of Molecular Oxygen by Manganese Porphyrins Supported on Ag(111)

Barry E. Murphy,[†] Sergey A. Krasnikov,[†,‡,*] Natalia N. Sergeeva,[§] Attilio A. Cafolla,[‡] Alexei B. Preobrajenski,[∥] Alexander N. Chaika,[†] Olaf Lübben,[†] and Igor V. Shvets[†]

[†]Centre for Research on Adaptive Nanostructures and Nanodevices (CRANN), School of Physics, Trinity College Dublin, Dublin 2, Ireland, [‡]School of Physical Sciences, Dublin City University, Glasnevin, Dublin 9, Ireland, [§]School of Chemistry, University of Leeds, Leeds LS2 9JT, U.K., and [∥]MAX-lab, Lund University, Box 118, S-22100 Lund, Sweden

ABSTRACT Oxygen binding and cleavage are important for both molecular recognition and catalysis. Mn-based porphyrins in particular are used as catalysts for the epoxidation of alkanes, and in this study the homolytic cleavage of O_2 by a surface-supported monolayer of Mn porphyrins on Ag(111) is demonstrated by scanning tunneling microscopy, X-ray absorption, and X-ray photoemission. As deposited, {5,10,15,20-tetraphenylporphyrinato}Mn(III)Cl (MnClTPP) has a flat orientation with its macrocycle parallel to the substrate and the axial Cl ligand pointing upward, away from the substrate. The adsorption of MnClTPP on Ag(111) is accompanied by a reduction of the Mn oxidation state from Mn(III) to Mn(II) due to charge transfer between the substrate and the molecule. Annealing the Mn(II)ClTPP monolayer up to 510 K causes the chlorine ligands to desorb from the porphyrins while leaving the monolayer intact. The Mn(II)TPP is stabilized by the surface acting as an axial ligand for the metal center. Exposure of the Mn(II)TPP/Ag(111) system to molecular oxygen results in the dissociation of O_2 and forms pairs of Mn(III)OTPP molecules on the surface. Annealing at 445 K reduces the Mn(III)OTPP complex back to Mn(II)TPP/Ag(111). The activation energies for Cl and O removal were found to be 0.35 ± 0.02 eV and 0.26 ± 0.03 eV, respectively.

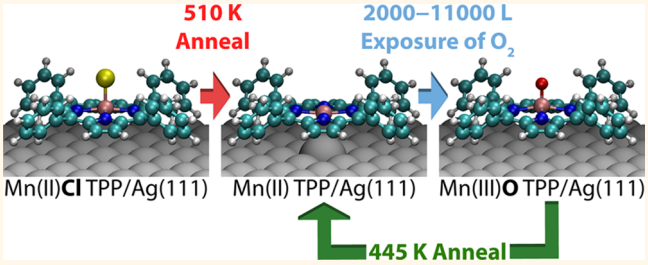

KEYWORDS: porphyrins · axial ligand · self-assembly · scanning tunneling microscopy · X-ray absorption · X-ray photoemission

Control over molecules on the atomic scale is routine in nature, for without it hemoglobin could not transport oxygen and almost all other biological processes would be impossible. However, such precise manipulation of matter on the smallest scale is still some way off for humanity. Considerable research has been focused on this issue for the past 50 years,[1−5] and with the advent of scanning probe microscopy and other highly local techniques, great strides have been made in the fields of atomic-scale manipulation,[6−11] molecular electronics,[12−16] and molecular structure determination.[17−20]

Three-dimensional (3D) transition metal (TM) porphyrins have featured widely in recent research due to their rich coordination chemistry, making them promising candidates for a large number of applications such as catalysis, nonlinear optics, enzyme models, sensors and molecular electronics.[21−24] Learning from nature, many biomimetic systems based on 3D TM porphyrins have been studied[22] and adapted for use in oxidation reactions.[23] In particular, manganese porphyrin complexes have been shown to selectively catalyze the halogenation of C−H bonds[25] and are often used as catalysts for the chemical transformation of alkenes into epoxides.[26,27] Given the ability of porphyrins to bind and release gases and to act as an active center in catalytic reactions in biological systems, porphyrin-based films on surfaces are extremely appealing as chemical and gas sensors as well as nanoporous catalytic materials.[23,28]

In the present work, scanning tunneling microscopy (STM), X-ray absorption (XA), X-ray photoemission spectroscopy (XPS), and density functional theory (DFT) calculations have been employed to study the self-assembly and central ligand transformation of {5,10,15,20-tetraphenylporphyrinato}Mn(III)Cl

* Address correspondence to sergey.krasnikov@dcu.ie.

Received for review March 3, 2014 and accepted April 26, 2014.

Published online 10.1021/nn501240j

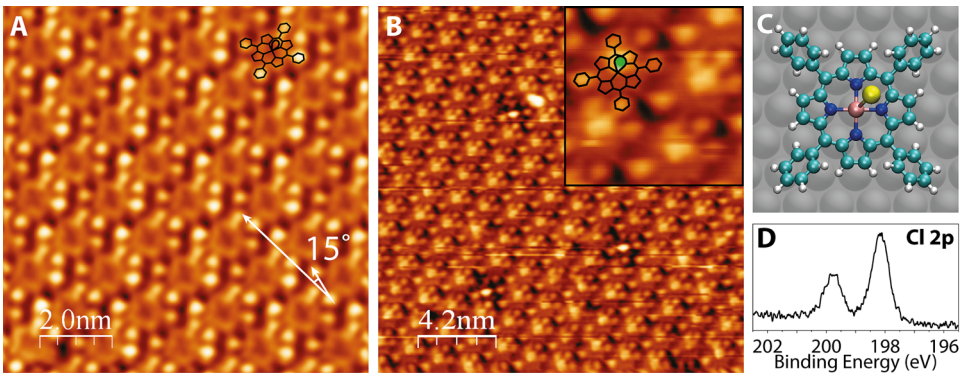

Figure 1. (A, B) STM images of 1 ML of MnClTPP. Depending on the bias chosen, the center of the molecules appears dark (A, $V_{sample} = -1.4$ V, $I_t = 0.3$ nA), or they have a bright protrusion (B, $V_{sample} = 2.0$ V, $I_t = 0.2$ nA) corresponding to the central Cl ligand. Inset in (B) shows an expanded region of several MnClTPP molecules with the molecular model overlaid. The arrows in (A) show the 15 ± 2° rotation of the molecules (short arrow) with respect to the close-packed direction of the monolayer (long arrow). (C) DFT model of MnClTPP on Ag(111), with the Cl ion (yellow) displaced from its optimal on-top position for clarity. (D) Cl 2p XPS measured from 1 ML of MnClTPP at incident photon energy of 300 eV.

(MnClTPP) on the Ag(111) surface. The results of this work demonstrate the physical manipulation of an axial bond through the application of heat, charge transfer from the substrate to the molecule, and the stabilizing effect of the underlying Ag(111) surface on the oxidation state of the central TM ion and the porphyrin itself. The reversible oxidation and reduction of the central ion by gaseous O_2 demonstrated here paves the way for future studies on the applicability of MnClTPP in gas sensing or catalytic applications.

RESULTS AND DISCUSSION

When deposited onto the Ag(111) surface at room temperature (RT), the MnClTPP molecules self-assemble at a monolayer (ML) coverage into a close-packed layer (Figure 1A and B) with a square packing geometry and a lattice parameter of 1.41 ± 0.05 nm. Occupied-state STM images of the MnClTPP monolayer obtained at negative sample biases (Figure 1A) show the molecules as four bright protrusions corresponding to the phenyl rings. These surround the porphyrin core, which appears as a darker ring with a dark center. This is consistent with previous studies of metalloporphyrins showing that the highest occupied molecular orbitals are mostly localized on the phenyl rings.[29−36] Furthermore, the rotated position of the phenyl rings makes them topologically higher than the porphyrin macrocycle.[29−33,37,38] A rotational angle of 58° ± 1° between the phenyl rings and the macrocycle plane is predicted by DFT calculations of a single molecule on the surface, and a schematic model of MnClTPP on Ag(111) is shown in Figure 1C, with the Cl ion displaced from its optimal position to show the underlying Mn center. When the unoccupied states of the molecules are probed at specific positive sample biases above 1.8 V (Figure 1B), the molecules show a bright protrusion in the center corresponding to the Cl ligand pointing out of the surface (green oval in inset). This is a direct confirmation that the MnClTPP molecules arrive at the Ag(111) surface with the Cl ligand intact. This is further confirmed by the presence of the Cl 2p doublet in the corresponding XPS taken from 1 ML of MnClTPP (Figure 1D).

The supramolecular ordering of a deposited porphyrin overlayer is mostly triggered by the side groups on the molecule. Indeed, a similar packing scheme with the same geometry has previously been reported for tetraphenyl-porphyrins (TPPs) with different metal centers on noble metal surfaces: MnCl-, Co-, and Fe-TPP on Ag(111)[29−31,33] and Ni-, Cu-, and Co-TPP on Au(111).[32] The MnClTPP molecules on Ag(111) are rotated by 15 ± 2° with respect to the close-packed directions of the monolayer. Such a rotation allows the phenyl rings of adjacent molecules to interact in the so-called "T-shape" configuration, where the edge of one phenyl ring is directed toward the π-cloud on the face of its neighboring phenyl ring.[39] This accounts for the strongly attractive interaction between molecules and plays a major role in their self-assembly. A similar process has been noted to play a key role in both biological and chemical recognition and the interactions between the aromatic side-chains of proteins.[40−42]

Also noted in the STM images is some "buckling" in the monolayer. This is illustrated in Figure 2A, where the purple and green arrows (or dots) point to phenyl rings with inequivalent heights on opposite sides of the same molecule. In this way one phenyl ring (purple) on each molecule is higher than the other three (green), and the side on which this occurs alternates along molecular rows. This is clearly visible in Figure 2B, which shows two line profiles taken across all the phenyl rings of two adjacent molecules, which are indicated by dashed rectangles in Figure 2A. In order to compare the two line profiles in Figure 2B, they are shifted by 25 pm relative to each other. Both line profiles show that one phenyl ring of each molecule is higher than the other three by almost 50 pm, while

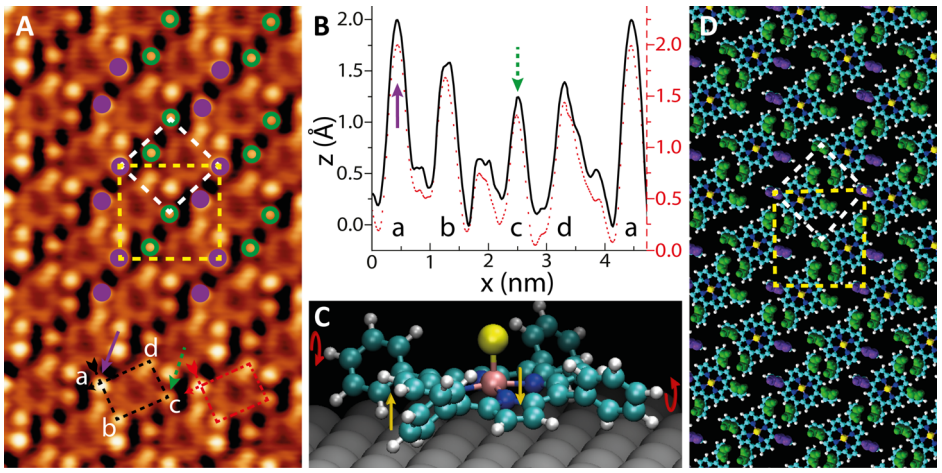

Figure 2. (A) STM of 1 ML of MnClTPP, illustrating the different rotational angles of phenyl rings attached to the same macrocycle. The white dotted square shows the primitive 1 × 1 unit cell, while the yellow dotted square shows the $\sqrt{2} \times \sqrt{2}$ *R*45° unit cell. The purple solid dots and arrows highlight the "upper" phenyl rings, while green open dots and dashed arrows correspond to the "lowest" phenyl rings of the molecules. (B) Line profiles across all phenyl rings of two adjacent molecules indicated by dashed rectangles in A. An offset of 25 pm between the line profiles is made for clarity. (C) Model of an isolated MnClTPP molecule relaxed on Ag(111) using DFT showing the *trans* arrangement of the phenyl rings. Yellow arrows highlight the saddling of the macrocycle, while the red arrows show the rotation of the phenyl rings. (D) Schematic model of the MnClTPP monolayer. The uppermost atoms of the phenyl rings are highlighted, with one phenyl ring of each molecule shown in purple to indicate the $\sqrt{2} \times \sqrt{2}$ ordering.

the height difference between the three lower phenyl rings does not exceed 20 pm. This buckling of the monolayer can be described by a $\sqrt{2} \times \sqrt{2}$ *R*45° unit cell shown in yellow in Figure 2A. It is noted that the $\sqrt{2} \times \sqrt{2}$ *R*45° unit cell is the smallest cell commensurate with the Ag(111) surface, with the corner molecules situated directly above a substrate atom and the central molecule situated on a bridge site between two Ag atoms.[29] It is unclear whether this "buckling" is caused by the plane of some molecules deviating from a parallel orientation with the surface or by one phenyl ring of each molecule being tilted almost perpendicular to the molecular plane. However, from previous studies of porphyrin complexes on noble metals,[30,32,33] and the strength of the interaction between such molecules and the surface, it is suggested that the latter is the case.

The interaction between the π-system of the macrocycle and the substrate has already been mentioned, and its significance is seen in the fact that the molecular unit cell and the axes of the molecules themselves are aligned along close-packed directions of the surface. It is therefore clear that the strength of this interaction is much larger than the energy required to rotate one phenyl ring around a single C−C bond. We propose that the molecules adopt this orientation in order to relieve some strain on the molecular layer and to facilitate a closer edge−face interaction between neighboring phenyl rings.

In order to identify the model for the molecular overlayer on the Ag(111) surface, DFT calculations have been performed. The phenyl rings have an axis of rotation around the single C−C bond joining them to the macrocycle. In order to match the molecular appearance from STM images, phenyl rings on adjacent sides of the molecule were rotated in opposite directions. We refer to this as the "*trans*" conformation, shown in Figure 2C, distinct from the "*cis*" conformation, where all four phenyl rings are rotated in the same direction (not shown here). This "counter-rotation" gives rise to some steric hindrance due to the proximity of the phenyl rings to the pyrrole rings of the porphyrin center. In turn, the macrocycle adopts a saddle conformation in order to increase the π-electron coupling between the phenyl rings and the porphyrin macrocycle,[43] with the outer carbon and hydrogen atoms of the adjacent pyrrole rings being pushed in opposite directions, into or out of the plane of the molecule.

Since the occupied state STM images of MnClTPP molecules taken at low bias voltages are dominated by protrusions of different brightness corresponding to the adjacent phenyl rings, these features are used to support the saddling hypothesis. It is clear from Figure 2D that the brightest (upper) portions of the phenyl rings are not evenly spaced around the periphery of the molecule, as they would be in the *cis* phenyl conformation. Instead, the bright protrusions are arranged at the corners of a rectangle, implying that the upper parts of the phenyl rings are tilted toward one another along the short side of the rectangle. This conformation is supported by DFT calculations, with the saddle-shaped *trans* molecule (Figure 2C) having a total energy 5 meV/atom lower than the planar *cis* conformation. As shown in the schematic comparison between the STM image in Figure 2A and the model in Figure 2D, this *trans* conformation reproduces the packing of the molecules very well, with the uppermost

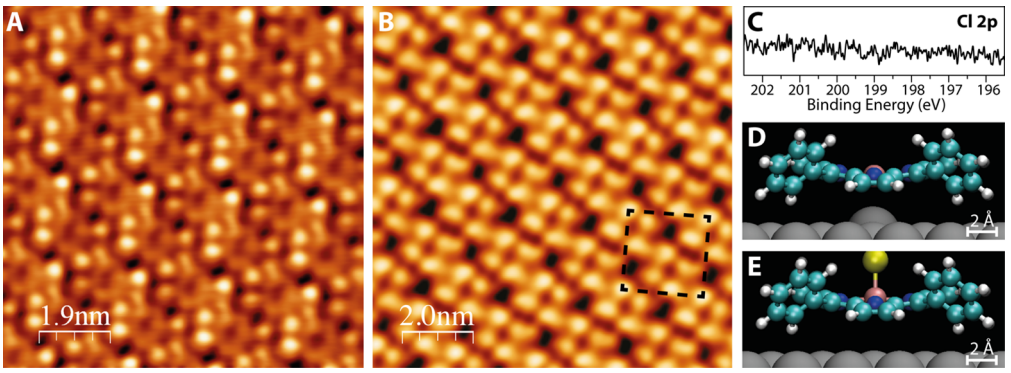

Figure 3. (A, B) STM images of 1 ML of MnTPP after annealing to 510 K. The occupied state image (A, $V_{sample} = -1.4$ V, $I_t = 0.3$ nA) appears unchanged from the case of the MnClTPP monolayer (Figure 1A); however in the unoccupied state images (B, $V_{sample} = 2.0$ V, $I_t = 0.2$ nA), the molecules have dark centers, where the Cl ligand was previously visible. The $\sqrt{2} \times \sqrt{2}$ *R*45° unit cell is shown in black. (C) Cl 2p XPS measured from 1 ML of MnTPP at an incident photon energy of 300 eV. (D, E) Relaxed models calculated for MnTPP (D) compared to MnClTPP (E) on Ag(111). After the Cl ligand is removed, the central Mn ion is situated closer to the surface, and an Ag atom is pulled upward toward the Mn, thus forming an axial ligand for the transition metal and stabilizing the MnTPP.

parts of the phenyl rings highlighted, as these are the brightest features on the STM image due to their proximity to the tip.

Annealing of the MnClTPP ML at 510 K leads to the complete removal of the Cl ligand. STM images obtained after such annealing are shown in Figure 3. The occupied-state images of MnTPP (Figure 3A) are almost identical to that of MnClTPP prior to annealing. The four phenyl rings are still visible, and the center of the macrocycle appears dark, as in Figure 1A. It is noted that the monolayer exhibits a square primitive lattice with an unchanged lattice parameter of 1.41 ± 0.05 nm. The rectangular arrangement of the phenyl rings is also unchanged, implying that the removal of the axial ligand does not greatly affect the *meso*-aryl substituents. However, when the unoccupied states are probed (Figure 3B), the appearance of the molecules is strikingly different.

The central protrusion seen in the images of the unannealed monolayer is now gone, providing evidence for the removal of the Cl ligand. Instead, the molecules appear as four large protrusions, corresponding to the positions of the phenyl substituents. The absence of Cl is further confirmed by the Cl 2p XPS measured from the monolayer after annealing to 510 K (Figure 3C). The $\sqrt{2} \times \sqrt{2}$ *R*45° supramolecular ordering is retained and visible in both the occupied- and unoccupied-state images, suggesting that it is topological in nature (*i.e.*, a rotation of one phenyl ring out of the surface); however in the latter case it is less pronounced.

In order to examine the behavior of the molecules after the Cl ligand is removed, an MnTPP molecule on Ag(111) was simulated by DFT. The fully relaxed model is shown in Figure 3, along with the relaxed model of the MnClTPP/Ag(111) system. As can be seen from the side-views in Figure 3D and E, the removal of the Cl ligand has little effect on the porphyrin macrocycle and its phenyl substituents, consistent with STM images. The Mn center in MnTPP, however, is situated 3.4 pm closer to the Ag(111) surface, and in turn the Ag atom directly below the Mn ion is pulled out of the surface toward the molecule by 8.7 pm. This result indicates that the Mn is coordinated by the Ag(111) surface, which acts as an axial ligand for the Mn ion, stabilizing the porphyrin.[28,29] A similar proximity of the central 3D TM atom to the underlying surface has been observed for monolayers of Fe and Co tetraphenylporphyrins on the Ag(111) surface.[44]

After removing the Cl ligand from the molecules, the resulting MnTPP/Ag(111) was exposed to molecular oxygen for various lengths of time in order to study the effect of oxidation on the molecular layer. STM images recorded after 15, 30, and 90 min oxygen exposure at a partial pressure of 2×10^{-6} mbar are shown in Figure 4. The lattice parameters of the ML are unchanged from those of MnClTPP and MnTPP, consistent with observations that the *meso*-aryl substituents are the main factors in supramolecular ordering.[33] It is observed that some molecules exhibit a very bright center, and the number of these molecules increases with oxygen exposure. Furthermore, it has been found that the oxidation usually proceeds by oxidizing pairs of neighboring molecules on the surface (see Figure 4A and B), so it is reasonable to assume that the O_2 dissociates, resulting in MnOTPP complexes. A similar scenario has been observed for the MnCl-porphyrins on Au(111) and HOPG surfaces in STM experiments performed at a liquid−solid interface.[20,28] It was found that Mn porphyrins in solution can bind and cleave O_2, which results in Mn(IV)═O species.[20,28] However, it has also been observed that the yield of oxidized manganese porphyrins was only in the range 10−20%, and a higher number of reacted molecules led to a decomposition of the molecular layer.[20,28,45]

To test the correlation between the oxidation of one molecule at the same time as one or more of its

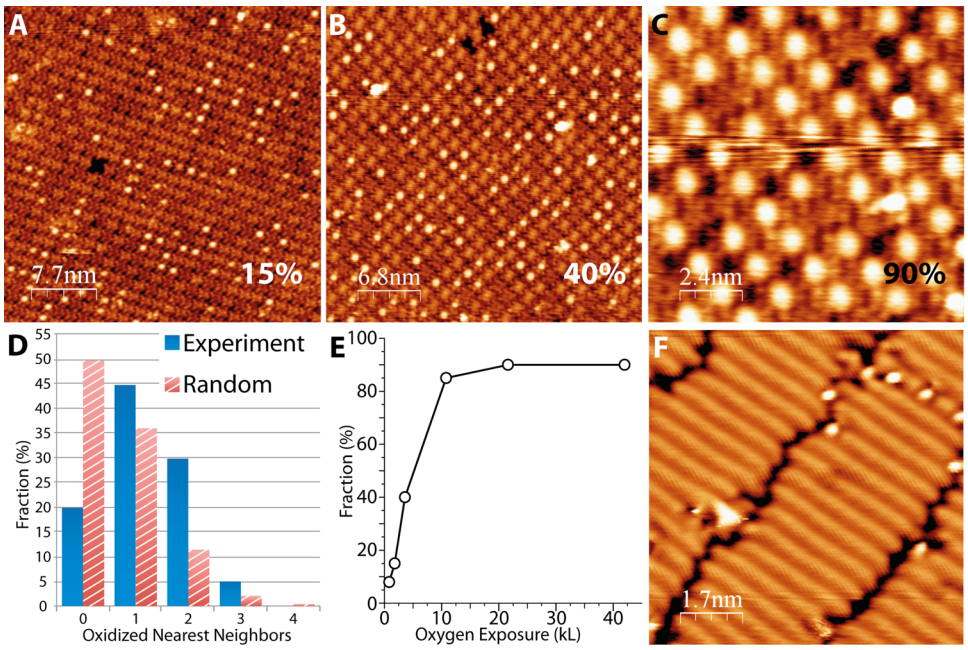

Figure 4. STM images of 1 ML of MnOTPP after various oxygen exposures: (A) 15 min (1800 L) with ~15% of the molecules oxidized; (B) 30 min (3600 L), ~40% oxidized; (C) 90 min (10 800 L), ~90% oxidized. $V_{sample} = -1.4$ V, $I_t = 0.3$ nA in each case. (D) Statistical distribution of the probability that an oxidized molecule has one or more nearest neighbors that are also oxidized (blue), compared to a binomial (random) distribution for the case of uncorrelated oxidation (red). Images with ~8% oxidized molecules were used for the statistical analysis. (E) Dependence of the fraction of oxidized molecules on oxygen exposure. (F) STM image of a region of the oxidized Ag(111) surface free of molecules after several oxidation–reduction cycles, $V_{sample} = -1.5$ V, $I_t = 0.7$ nA.

neighbors, the number of oxidized nearest neighbors for a large number of oxidized molecules (~2000 molecules in total) was counted, as shown in blue in Figure 4D. This analysis has been performed using STM images of the molecular layer exposed to 840 L of O_2 (~8% fraction of oxidized molecules). If the oxidation were to follow an uncorrelated, random pattern, *i.e.*, each molecule becomes oxidized independently of its neighbors, forming MnO_2TPP, then the number of oxidized molecules in the monolayer would have a binomial distribution at any given time.[28] The binomial distribution corresponding to the same fraction of oxidized molecules as the experimental data (8%) is shown in Figure 4D in red. It is clear that the number of oxidized nearest neighbors in our experiment is correlated, implying that when one porphyrin becomes oxidized, its neighbor has an increased chance of oxidizing. This supports the theory that the MnTPP/Ag(111) system causes the O_2 molecule to undergo homolytic cleavage, and the free O atoms are likely to bond with two neighboring MnTPP molecules.

Since this experiment has been performed under UHV conditions, it emphasizes the role of the substrate in O_2 cleavage by MnTPP/Ag(111). The O_2 dissociation upon reaction with the MnTPP is facilitated by the Ag(111) surface, from which an atom coordinates to the Mn as an axial ligand (Figure 3D). Furthermore, in the case of the MnTPP/Ag(111) system, the number of molecules within the monolayer that have reacted with oxygen reaches 90% (see Figure 4C). This is explained by the stability of the layer due to a significant interaction between the molecules and the substrate. Such an interaction prevents neighboring molecules from leaving their place in the layer to go on top of each other and form porphyrin dimers bonded through an O axial ligand. These dimers have been observed in STM experiments performed in solution and negatively affect the catalytic properties of the porphyrin layer, leading to its destruction.[20,45]

The percentages shown on the STM images in Figure 4 indicate the amount of MnTPP molecules that have been converted to the MnOTPP state. After exposures of 90 min (10 800 L) or more, approximately 90% of the molecules are converted to MnOTPP. However, at this point the oxidation appears to saturate, as the dependence of the fraction of oxidized molecules on oxygen exposure (Figure 4E) demonstrates. The logarithmic dependence and saturation of the oxidation process indicate that it is self-limiting and that only MnTPP molecules not yet converted to the MnOTPP state can cleave molecular oxygen. The number of unconverted molecules decreases with exposure, proving that oxygen atoms are trapped by the molecules after cleavage. The MnOTPP molecule on the Ag(111) surface was also simulated using DFT. The relaxed structure of MnOTPP (not shown here) exhibits a saddling of the molecule, similar to MnClTPP and MnTPP, with the oxygen atom of the lowest-energy structure pointing away from the surface, similar to the chlorine on MnClTPP.

It was found that annealing the MnOTPP monolayer up to 445 K results in the desorption of oxygen bound to the molecules without disturbing the structure of the monolayer, and STM images of MnTPP identical to those presented in Figure 3 were obtained (not shown here). Several oxidation and reduction cycles of the MnTPP/Ag(111) were performed without destroying the molecular overlayer. However, patches of oxidized Ag surface have been observed to form with time (Figure 4F). It is known that the Ag(111) can be oxidized by O_2 through its dissociation only at very high oxygen pressure and surface temperatures.[46] Therefore, such an observation confirms that the O_2 is cleaved by MnTPP/Ag(111), leading to MnOTPP/Ag(111). Annealing the latter releases oxygen atoms, which either react with each other to form O_2 or oxidize the substrate.

In order to explore changes in the oxidation state of the central Mn ion at each step of the experiment, Mn 2p X-ray absorption spectroscopy has been performed. The Mn $2p_{3/2}$ (L_3) XA spectra consist of three main features, labeled A, B, and C in Figure 5. These structures result from transitions of the core $2p_{3/2}$ electrons to the outer valence states and have been shown to reflect the oxidation state of the Mn ion.[47,48] However, the decomposition of such spectra is complex,[47,48] and so here the main features will be treated as a "fingerprint" of the oxidation state. When the Mn ion is in the II oxidation state (MnO, Figure 5, curve 2), the B feature dominates, with a significant contribution from A and a lower shoulder at C. In the Mn(III) state (Mn_2O_3, Figure 5, curve 1), the contribution of the C feature dominates. In the case of a thick MnClTPP layer (Figure 5, curve 3), the Mn $2p_{3/2}$ XA spectrum is similar to that measured from a thick layer of the Mn(III)Cl-octaethyl-porphyrin[49] and has a shape characteristic of the Mn(III) oxidation state.[47,48] In turn, the Mn $2p_{3/2}$ XA spectrum of the as-deposited monolayer (Figure 5, curve 4) exhibits a shape characteristic of the Mn(II) oxidation state, very similar to MnO and other Mn(II) compounds.[47,48] This is clear evidence that there is a significant charge transfer (approximately one electron) from the substrate to the porphyrin upon adsorption of the molecules, resulting in the formation of the Mn(II)ClTPP/Ag(111) system. Such a reduction of the Mn oxidation state from III to II in the case of 1 ML cannot be accounted for by the loss of the Cl axial ligand since the molecules stay intact, as observed by STM and Cl 2p XPS (see Figure 1).

When the Mn(II)ClTPP/Ag(111) is annealed at 510 K, the Cl ligand is removed, as confirmed by STM and the Cl 2p XPS. However, from the shape of the Mn $2p_{3/2}$ XA (Figure 5, curve 5) it is clear that the oxidation state of the Mn ion is unchanged. Without the Cl ligand, the Mn ion would be undercoordinated by the porphyrin macrocycle alone. This supports the finding from DFT calculations that the Ag(111) surface is indeed acting as an axial ligand and stabilizing the Mn(II) oxidation state of the Mn ion center.[20,28,29]

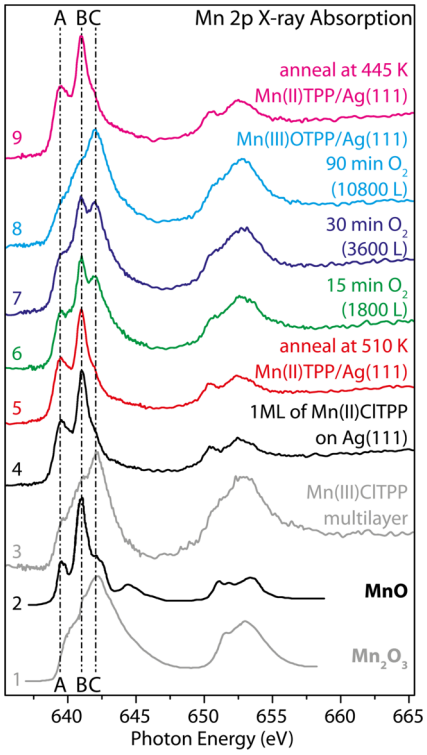

Figure 5. Mn 2p XA spectra acquired during the anneal and subsequent oxygen exposure of the MnClTPP monolayer on Ag(111), compared to the MnClTPP multilayer spectrum and reference spectra from Mn_2O_3 and MnO.[48] In the case of a multilayer (curve 3), the Mn $2p_{3/2}$ peaks have a shape characteristic of the Mn(III) oxidation state. When 1 ML is deposited (curve 4), the Mn oxidation state changes to Mn(II) due to substrate−molecule charge transfer, resulting in Mn(II)ClTPP/Ag(111). This is preserved upon annealing at 510 K to yield Mn(II)TPP/Ag(111) (curve 5). Upon exposure to O_2, the central Mn changes its oxidation state from Mn(II) to Mn(III) (curves 6−8), leading to Mn(III)OTPP/Ag(111). The Mn(II)TPP/Ag(111) system can then be regenerated by further annealing at 445 K (curve 9), causing desorption of the oxygen.

Upon subsequent exposure of the Mn(II)TPP/Ag(111) complex to O_2, the Mn $2p_{3/2}$ line shape changes significantly. As oxidation time increases, the relative contributions of the A and B features diminish, and the C peak gradually grows to be the principal feature. This implies that exposure to oxygen causes the Mn ion to change from the II oxidation state to the III. The Mn $2p_{3/2}$ XA spectra were measured after exposure to the same doses of O_2 as the samples shown in Figures 4A−C, with spectrum 6 (1800 L of O_2) corresponding to approximately 15% of the molecules oxidized, spectrum 7 (3600 L), 40%, and spectrum 8 (10800 L), 90%. The Mn oxidation is reversible, and further annealing at 445 K removes the oxygen axial ligand, restoring the Mn(II) line shape (Figure 5, spectrum 9).

In order to measure the activation energy required to initiate the desorption of the Cl axial ligand, Cl 2p XPS were recorded from the MnClTPP monolayer as it was annealed. The spectra presented in Figure 6A were measured while the temperature was gradually

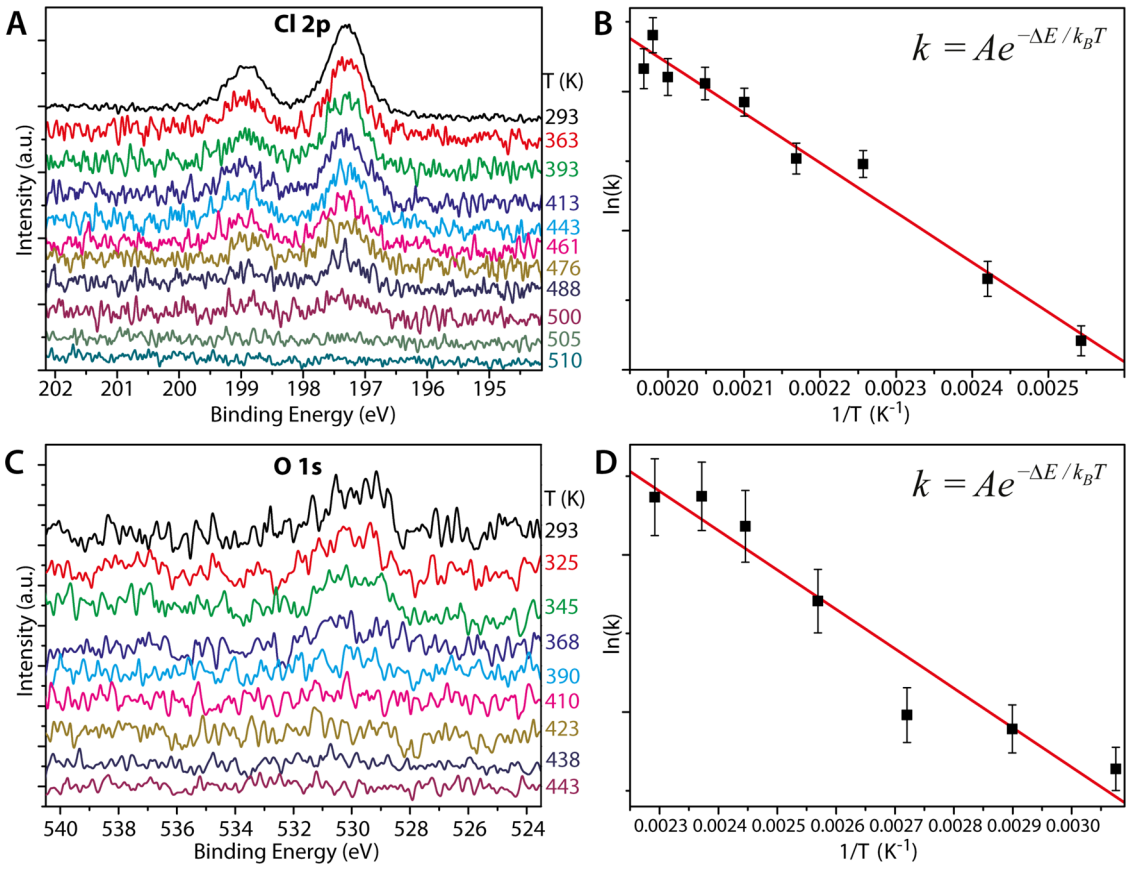

Figure 6. (A) Cl 2p XPS measured at an excitation energy of 300 eV while annealing the Mn(II)ClTPP/Ag(111) at varying temperatures (shown on the right-hand side of graph). (B) Arrhenius plot of the logarithm of the Cl peak intensity *vs* the reciprocal of the temperature, giving an activation energy for the desorption of Cl of $\Delta E_{Cl} = 0.35 \pm 0.02$ eV. (C) O 1s XPS measured at an excitation energy of 620 eV during the anneal of the Mn(III)OTPP/Ag(111) system (temperature in K shown on right-hand side). (D) Arrhenius plot of the logarithm of the O peak intensity *vs* the reciprocal of the temperature, giving an activation energy for the desorption of O of $\Delta E_O = 0.26 \pm 0.03$ eV. The error bars in B and D are based on the error in the areas of XPS peaks determined from the uncertainty in the peak-fitting procedure.

increased, with the temperature shown on the right of the plots. It is observed that at around 510 K the Cl 2p doublet is reduced to the level of the background noise. The experiment was performed with a constant heating rate of 10 K/min, and so the difference in area between two spectra can be used in an Arrhenius analysis to derive the rate of Cl desorption, $k = A\, e^{-\Delta E/k_BT}$. A plot of ln($k$) *vs* 1/$T$ is presented in Figure 6B. The slope of the best-fit line gives a value for the activation energy of $\Delta E_{Cl} = 0.35 \pm 0.02$ eV.

The same procedure has been applied to obtain the activation energy for the desorption of the O axial ligand from the molecules. The O 1s spectra are presented in Figure 6C, with the temperature at which each spectrum was recorded shown at the right side. The shape and the energy position of the O 1s peak measured from the oxidized monolayer at RT (Figure 6C, top spectrum) are similar to those for chemisorbed atomic oxygen on the Mn/Pd(100) surface.[50] This further confirms the O_2 dissociation and formation of the Mn(III)OTPP/Ag(111) complex. The same heating rate as for Cl desorption of 10 K/min was used. The O 1s XPS data were treated similarly to the Cl 2p data, and Figure 6D shows the Arrhenius plot for oxygen desorption. In this case, the activation energy for the desorption of O was found to be $\Delta E_O = 0.26 \pm 0.03$ eV.

CONCLUSION

In summary, STM, XA, XPS, and DFT were used to study the self-assembly and the central ligand transformation of a surface-supported monolayer of (5,10,15,20-tetraphenylporphyrinato)Mn(III)Cl (MnClTPP). When deposited onto the Ag(111) surface, MnClTPP molecules self-assemble into large well-ordered molecular domains. Each molecule adopts a saddle conformation with the axial Cl ligand pointing out of the plane of the molecule into the vacuum. One phenyl ring of each molecule is rotated slightly closer to the surface normal, giving rise to a $\sqrt{2} \times \sqrt{2}\, R45°$ molecular Bravais unit cell. Upon adsorption, the Mn oxidation state is reduced from Mn(III) to Mn(II) due to charge transfer between the substrate and the molecule.

Annealing the Mn(II)ClTPP/Ag(111) up to 510 K causes the Cl axial ligand to desorb from the porphyrin while leaving the supramolecular order and Mn(II)

oxidation state unaffected. The Mn(II)TPP is stabilized by the Ag(111) surface acting as an axial ligand for the metal center. When the Mn(II)TPP/Ag(111) complex is exposed to molecular oxygen, the latter dissociates, forming O axial ligands and changing the oxidation state of the central Mn from II to III. Further annealing at 445 K reduces the Mn(III)OTPP/Ag(111) complex back to Mn(II)TPP/Ag(111). The activation energies for Cl and O removal, derived from the XPS data, were found to be 0.35 ± 0.02 eV and 0.26 ± 0.03 eV, respectively.

METHODS

The STM experiments were performed at 78 K in an ultra-high-vacuum system consisting of an analysis chamber (with a base pressure of 2×10^{-11} mbar) and a preparation chamber (5×10^{-11} mbar). An electrochemically etched [100]-oriented single-crystalline W tip[51,52] was used to record STM images in constant-current mode. Due to the high stability of this tip,[52] 90% of the STM images recorded were similar to the ones shown in this work. The voltage V_{sample} corresponds to the sample bias with respect to the tip. STM topographic images were processed using WSxM software.[53] No drift corrections have been applied to any of the STM images presented.

The Ag(111) crystal (Surface Preparation Laboratory) was cleaned *in situ* by repeated cycles of argon ion sputtering (E_k = 0.8 keV) and annealing at 820 K. The substrate cleanliness was verified by STM and LEED before deposition of the MnClTPP. MnClTPP was synthesized according to a published procedure.[28,54] The molecules were evaporated in a preparation chamber isolated from the STM chamber at a rate of approximately 0.2 ML per minute from a tantalum crucible in a home-made deposition cell operated at a temperature of approximately 600 K. The total pressure during porphyrin deposition was in the 10^{-10} mbar range. Before evaporation, the MnClTPP powder was degassed for about 2 h to remove water vapor.

XA and XPS measurements were performed at the D1011 beamline at MAX II storage ring in Lund, Sweden, with an identical sample preparation procedure as for the STM experiments. The XPS spectra were measured with a Scienta SES-200 electron energy analyzer. The kinetic energy resolution was set to 100 and 300 meV for the Cl 2p and O 1s spectra, respectively. The XA spectra were recorded in the partial electron yield mode ($U = -300$ V) by a multichannel plate detector and normalized to the background curves recorded from the clean substrate. The photon energy resolution was set to 150 meV at the Mn L_3-edge (~640 eV).

DFT calculations were performed using the Vienna *Ab Initio* Simulation Package (VASP) program. VASP implements a projected augmented basis set (PAW)[55] and periodic boundary conditions. The electron exchange and correlation was simulated by generalized gradient approximation (GGA) pseudopotentials with a Perdew–Burke–Ernzerhof (PBE) exchange–correlation density functional.[56] A single k-point (Γ) was used for all calculations to sample the Brillouin zone. The applied energy cutoff was 400 eV. The global break condition for the electronic self-consistent loops was set to a total energy change of less than 1×10^{-4} eV, and all conformations were fully relaxed (forces <0.01 eV/Å). In the calculations, four layers of Ag were used; with the lower two constrained to simulate the bulk. The molecules were placed on top of the Ag(111) surface and allowed to relax along with the top two layers of Ag. A vacuum slab of 10 Å was used to separate the system from its translational images.

Conflict of Interest: The authors declare no competing financial interest.

Acknowledgment. This work was supported by Science Foundation Ireland through the Principal Investigator grants (SFI P.I. 09/IN.1/I2635 and SFI P.I. 12/IA/1264).

REFERENCES AND NOTES

1. Stroscio, J. A.; Eigler, D. M. Atomic and Molecular Manipulation with the Scanning Tunneling Microscope. *Science* **1991**, *254*, 1319–1326.
2. Rosei, F.; Schunack, M.; Naitoh, Y.; Jiang, P.; Gourdon, A.; Lægsgaard, E.; Stensgaard, I.; Joachim, C.; Besenbacher, F. Properties of Large Organic Molecules on Metal Surfaces. *Prog. Surf. Sci.* **2003**, *71*, 95–146.
3. Smith, R. K.; Lewis, P. A.; Weiss, P. S. Patterning Self-Assembled Monolayers. *Prog. Surf. Sci.* **2004**, *75*, 1–68.
4. Barth, J. V.; Costantini, G.; Kern, K. Engineering Atomic and Molecular Nanostructures at Surfaces. *Nature* **2005**, *437*, 671–679.
5. Klappenberger, F. Two-Dimensional Functional Molecular Nanoarchitectures – Complementary Investigations with Scanning Tunneling Microscopy and X-Ray Spectroscopy. *Prog. Surf. Sci.* **2014**, *89*, 1–55.
6. Eigler, D. M.; Lutz, C. P.; Rudge, W. E. An Atomic Switch Realized with the Scanning Tunneling Microscope. *Nature* **1991**, *352*, 600–603.
7. Burema, S. R.; Seufert, K.; Auwaerter, W.; Barth, J. V.; Bocquet, M.-L. Probing Nitrosyl Ligation of Surface-Confined Metalloporphyrins by Inelastic Electron Tunneling Spectroscopy. *ACS Nano* **2013**, *7*, 5273–5281.
8. Kim, H.; Chang, Y. H.; Lee, S.-H.; Kim, Y.-H.; Kahng, S.-J. Switching and Sensing Spin States of Co-Porphyrin in Bimolecular Reactions on Au(111) Using Scanning Tunneling Microscopy. *ACS Nano* **2013**, *7*, 9312–9317.
9. Krasnikov, S. A.; Lübben, O.; Murphy, B. E.; Bozhko, S. I.; Chaika, A. N.; Sergeeva, N. N.; Bulfin, B.; Shvets, I. V. Writing with Atoms: Oxygen Adatoms on the MoO_2/Mo(110) Surface. *Nano Res.* **2013**, *6*, 929–937.
10. Sweetman, A.; Jarvis, S.; Danza, R.; Bamidele, J.; Gangopadhyay, S.; Shaw, G. A.; Kantorovich, L.; Moriarty, P. Toggling Bistable Atoms *via* Mechanical Switching of Bond Angle. *Phys. Rev. Lett.* **2011**, *106*, 136101.
11. Kumagai, T.; Hanke, F.; Gawinkowski, S.; Sharp, J.; Kotsis, K.; Waluk, J.; Persson, M.; Grill, L. Controlling Intramolecular Hydrogen Transfer in a Porphycene Molecule with Single Atoms or Molecules Located Nearby. *Nat. Chem.* **2014**, *6*, 41–46.
12. Joachim, C.; Gimzewski, J. K.; Aviram, A. Electronics Using Hybrid-Molecular and Mono-Molecular Devices. *Nature* **2000**, *408*, 541–548.
13. Zhu, X. Y. Electronic Structure and Electron Dynamics at Molecule-Metal Interfaces: Implications for Molecule-Based Electronics. *Surf. Sci. Rep.* **2004**, *56*, 1–83.
14. Auwärter, W.; Seufert, K.; Bischoff, F.; Écija, D.; Vijayaraghavan, S.; Joshi, S.; Klappenberger, F.; Samudrala, N.; Barth, J. V. A Surface-Anchored Molecular Four-Level Conductance Switch Based on Single Proton Transfer. *Nat. Nanotechnol.* **2012**, *7*, 41–46.
15. Bozhko, S. I.; Krasnikov, S. A.; Lübben, O.; Murphy, B. E.; Radican, K.; Semenov, V. N.; Wu, H. C.; Levchenko, E. A.; Chaika, A. N.; Sergeeva, N. N.; *et al.* Correlation between Charge-Transfer and Rotation of C60 on WO_2/W(110). *Nanoscale* **2013**, *5*, 3380–3386.
16. Garnica, M.; Stradi, D.; Barja, S.; Calleja, F.; Diaz, C.; Alcami, M.; Martin, N.; de Parga, A. L. V.; Martin, F.; Miranda, R. Long-Range Magnetic Order in a Purely Organic 2D Layer Adsorbed on Epitaxial Graphene. *Nat. Phys.* **2013**, *9*, 368–374.
17. Jung, T. A.; Schlittler, R. R.; Gimzewski, J. K. Conformational Identification of Individual Adsorbed Molecules with the STM. *Nature* **1997**, *386*, 696–698.
18. Ruan, L.; Besenbacher, F.; Stensgaard, I.; Lægsgaard, E. Atom-Resolved Discrimination of Chemically Different Elements on Metal-Surfaces. *Phys. Rev. Lett.* **1993**, *70*, 4079–4082.

19. Stipe, B. C.; Rezaei, H. A.; Ho, W. Localization of Inelastic Tunneling and the Determination of Atomic-Scale Structure with Chemical Specificity. *Phys. Rev. Lett.* **1999**, *82*, 1724–1727.
20. den Boer, D.; Li, M.; Habets, T.; Iavicoli, P.; Rowan, A. E.; Nolte, R. J. M.; Speller, S.; Amabilino, D. B.; de Feyter, S.; Elemans, J. A. Detection of Different Oxidation States of Individual Manganese Porphyrins during Their Reaction with Oxygen at a Solid/Liquid Interface. *Nat. Chem.* **2013**, *5*, 621–627.
21. de Montellano, P. R. O. *Cytochrome P450: Structure, Mechanism, and Biochemistry*; Springer: New York, 2005.
22. Feiters, M. C.; Rowan, A. E.; Nolte, R. J. From Simple to Supramolecular Cytochrome P450 Mimics. *Chem. Soc. Rev.* **2000**, *29*, 375–384.
23. Meunier, B. Metalloporphyrins as Versatile Catalysts for Oxidation Reactions and Oxidative DNA Cleavage. *Chem. Rev.* **1992**, *92*, 1411–1456.
24. Seufert, K.; Bocquet, M. L.; Auwärter, W.; Weber-Bargioni, A.; Reichert, J.; Lorente, N.; Barth, J. V. Cis-Dicarbonyl Binding at Cobalt and Iron Porphyrins with Saddle-Shape Conformation. *Nat. Chem.* **2011**, *3*, 114–119.
25. Liu, W.; Groves, J. T. Manganese Porphyrins Catalyze Selective C−H Bond Halogenations. *J. Am. Chem. Soc.* **2010**, *132*, 12847–12849.
26. Groves, J. T. Reactivity and Mechanisms of Metalloporphyrin-Catalyzed Oxidations. *J. Porphyrins Phthalocyanines* **2000**, *4*, 350–352.
27. Groves, J. T.; Nemo, T. E. Epoxidation Reactions Catalyzed by Iron Porphyrins. Oxygen Transfer from Iodosylbenzene. *J. Am. Chem. Soc.* **1983**, *105*, 5786–5791.
28. Hulsken, B.; Hameren, R. V.; Gerritsen, J. W.; Khoury, T.; Thordarson, P.; Crossley, M. J.; Rowan, A. E.; Nolte, R. J.; Elemans, J. A.; Speller, S. Real-Time Single-Molecule Imaging of Oxidation Catalysis at a Liquid−Solid Interface. *Nat. Nanotechnol.* **2007**, *2*, 285–289.
29. Beggan, J. P.; Krasnikov, S. A.; Sergeeva, N. N.; Senge, M. O.; Cafolla, A. A. Control of the Axial Coordination of a Surface-Confined Manganese (III) Porphyrin Complex. *Nanotechnology* **2012**, *23*, 235606.
30. Auwärter, W.; Seufert, K.; Klappenberger, F.; Reichert, J.; Weber-Bargioni, A.; Verdini, A.; Cvetko, D.; Dell'Angela, M.; Floreano, L.; Cossaro, A.; *et al*. Site-Specific Electronic and Geometric Interface Structure of Co-Tetraphenyl-Porphyrin Layers on Ag (111). *Phys. Rev. B* **2010**, *81*, 245403.
31. Comanici, K.; Buchner, F.; Flechtner, K.; Lukasczyk, T.; Gottfried, J. M.; Steinrück, H.-P.; Marbach, H. Understanding the Contrast Mechanism in Scanning Tunneling Microscopy (STM) Images of an Intermixed Tetraphenylporphyrin Layer on Ag(111). *Langmuir* **2008**, *24*, 1897–1901.
32. Scudiero, L.; Barlow, D. E.; Hipps, K. Physical Properties and Metal Ion Specific Scanning Tunneling Microscopy Images of Metal (II) Tetraphenylporphyrins Deposited from Vapor onto Gold (111). *J. Phys. Chem. B* **2000**, *104*, 11899–11905.
33. Buchner, F.; Kellner, I.; Hieringer, W.; Gorling, A.; Steinruck, H.-P.; Marbach, H. Ordering Aspects and Intramolecular Conformation of Tetraphenylporphyrins on Ag(111). *Phys. Chem. Chem. Phys.* **2010**, *12*, 13082–13090.
34. Krasnikov, S. A.; Sergeeva, N. N.; Brzhezinskaya, M. M.; Preobrajenski, A. B.; Sergeeva, Y. N.; Vinogradov, N. A.; Cafolla, A. A.; Senge, M. O.; Vinogradov, A. S. An X-Ray Absorption and Photoemission Study of the Electronic Structure of Ni Porphyrins and Ni N-Confused Porphyrin. *J. Phys.: Condens. Matter* **2008**, *20*, 235207.
35. Krasnikov, S. A.; Preobrajenski, A. B.; Sergeeva, N. N.; Brzhezinskaya, M. M.; Nesterov, M. A.; Cafolla, A. A.; Senge, M. O.; Vinogradov, A. S. Electronic Structure of Ni(II) Porphyrins and Phthalocyanine Studied by Soft X-Ray Absorption Spectroscopy. *Chem. Phys.* **2007**, *332*, 318–324.
36. Liao, M.-S.; Scheiner, S. Electronic Structure and Bonding in Metal Porphyrins, Metal=Fe, Co, Ni, Cu, Zn. *J. Chem. Phys.* **2002**, *117*, 205.
37. Krasnikov, S. A.; Sergeeva, N. N.; Sergeeva, Y. N.; Senge, M. O.; Cafolla, A. A. Self-Assembled Rows of Ni Porphyrin Dimers on the Ag(111) Surface. *Phys. Chem. Chem. Phys.* **2010**, *12*, 6666–6671.
38. Krasnikov, S. A.; Doyle, C. M.; Sergeeva, N. N.; Preobrajenski, A. B.; Vinogradov, N. A.; Sergeeva, Y. N.; Zakharov, A. A.; Senge, M. O.; Cafolla, A. A. Formation of Extended Covalently Bonded Ni Porphyrin Networks on the Au(111) Surface. *Nano Res.* **2011**, *4*, 376–384.
39. Jennings, W. B.; Farrell, B. M.; Malone, J. F. Attractive Intramolecular Edge-to-Face Aromatic Interactions in Flexible Organic Molecules. *Acc. Chem. Res.* **2001**, *34*, 885–894.
40. Brede, J.; Linares, M.; Kuck, S.; Schwoebel, J.; Scarfato, A.; Chang, S.-H.; Hoffmann, G.; Wiesendanger, R.; Lensen, R.; Kouwer, P. H.; *et al*. Dynamics of Molecular Self-Ordering in Tetraphenyl Porphyrin Monolayers on Metallic Substrates. *Nanotechnology* **2009**, *20*, 275602.
41. Meyer, E. A.; Castellano, R. K.; Diederich, F. Interactions with Aromatic Rings in Chemical and Biological Recognition. *Angew. Chem., Int. Ed.* **2003**, *42*, 1210–1250.
42. Burley, S.; Petsko, G. Aromatic-Aromatic Interaction: A Mechanism of Protein Structure Stabilization. *Science* **1985**, *229*, 23–28.
43. Rosa, A.; Ricciardi, G.; Baerends, E. J. Synergism of Porphyrin-Core Saddling and Twisting of *Meso*-Aryl Substituents. *J. Phys. Chem. A* **2006**, *110*, 5180–5190.
44. Hieringer, W.; Flechtner, K.; Kretschmann, A.; Seufert, K.; Auwärter, W.; Barth, J. V.; Görling, A.; Steinrück, H.-P.; Gottfried, J. M. The Surface Trans Effect: Influence of Axial Ligands on the Surface Chemical Bonds of Adsorbed Metalloporphyrins. *J. Am. Chem. Soc.* **2011**, *133*, 6206–6222.
45. Elemans, J. A. A. W.; Bijsterveld, E. J. A.; Rowan, A. E.; Nolte, R. J. M. Manganese Porphyrin Hosts as Epoxidation Catalysts − Activity and Stability Control by Axial Ligand Effects. *Eur. J. Org. Chem.* **2007**, *2007*, 751–757.
46. Campbell, C. T. Atomic and Molecular Oxygen Adsorption on Ag(111). *Surf. Sci.* **1985**, *157*, 43.
47. Gilbert, B.; Frazer, B. H.; Belz, A.; Conrad, P. G.; Nealson, K. H.; Haskel, D.; Lang, J. C.; Srajer, G.; de Stasio, G. Multiple Scattering Calculations of Bonding and X-Ray Absorption Spectroscopy of Manganese Oxides. *J. Phys. Chem. A* **2003**, *107*, 2839–2847.
48. Kang, J.-S.; Kim, G.; Lee, H. J.; Kim, D. H.; Kim, H. S.; Shim, J. H.; Lee, S.; Lee, H.; Kim, J.-Y.; Kim, B. H.; *et al*. Soft X-Ray Absorption Spectroscopy and Magnetic Circular Dichroism Study of the Valence and Spin States in Spinel $MnFe_2O_4$. *Phys. Rev. B* **2008**, *77*, 035121.
49. Cook, P. L.; Liu, X.; Yang, W.; Himpsel, F. J. X-Ray Absorption Spectroscopy of Biomimetic Dye Molecules for Solar Cells. *J. Chem. Phys.* **2009**, *131*, 194701.
50. Li, F.; Parteder, G.; Allegretti, F.; Franchini, C.; Podloucky, R.; Surnev, S.; Netzer, F. P. Two-Dimensional Manganese Oxide Nanolayers on Pd(100): the Surface Phase Diagram. *J. Phys.: Condens. Matter* **2009**, *21*, 134008.
51. Chaika, A. N.; Nazin, S. S.; Semenov, V. N.; Bozhko, S. I.; Lübben, O.; Krasnikov, S. A.; Radican, K.; Shvets, I. V. Selecting the Tip Electron Orbital for Scanning Tunnelling Microscopy Imaging with Sub-Ångström Lateral Resolution. *Europhys. Lett.* **2010**, *92*, 46003.
52. Chaika, A. N.; Orlova, N. N.; Semenov, V. N.; Postnova, E. Y.; Krasnikov, S. A.; Lazarev, M. G.; Chekmazov, S. V.; Aristov, V. Y.; Glebovsky, V. G.; Bozhko, S. I.; *et al*. Fabrication of [001]-Oriented Tungsten Tips for High Resolution Scanning Tunneling Microscopy. *Sci. Rep.* **2014**, *4*, 3742.
53. Horcas, I.; Fernández, R.; Gómez-Rodriguez, J. M.; Colchero, J.; Gómez-Herrero, J.; Baro, A. M. WSXM: A Software for Scanning Probe Microscopy and a Tool for Nanotechnology. *Rev. Sci. Instrum.* **2007**, *78*, 013705.
54. Adler, A. D.; Longo, F. R.; Kampas, F.; Kim, J. On the Preparation of Metalloporphyrins. *J. Inorg. Nucl. Chem.* **1970**, *32*, 2443–2445.
55. Kresse, G.; Furthmüller, J. Efficient Iterative Schemes for *Ab Initio* Total-Energy Calculations Using a Plane-Wave Basis Set. *Phys. Rev. B* **1996**, *54*, 11169–11186.
56. Perdew, J. P.; Burke, K.; Ernzerhof, M. Generalized Gradient Approximation Made Simple. *Phys. Rev. Lett.* **1996**, *77*, 3865.